Attachment 14
PG&E Letter DCL-14-028

AREVA Calculation No. 32-9219792-000

Diablo Canyon Unit 2 Pressurizer Spray Nozzle Weld Overlay Residual Stress Analysis – Non-Proprietary

AREVA

CALCULATION SUMMARY SHEET (CSS)

Document No. 32 - 9219792 - 000 Safety Related: ☒Yes ☐ No

Title Diablo Canyon Unit 2 Pressurizer Spray Nozzle Weld Overlay Residual Stress Analysis – Non-Proprietary

PURPOSE AND SUMMARY OF RESULTS:

The purpose of this report is to document the weld residual stress finite element analysis of the pressurizer spray nozzle of Diablo Canyon Unit 2 in support of the planned preemptive mitigation of primary water stress corrosion cracking (PWSCC) susceptible Alloy 82/182 dissimilar metal welds using PWSCC resistant **[ ]** full structural weld overlays (SWOL). The state of residual stresses at shutdown (70F) and steady state (**[ ]** F) after the completion of the SWOL, as predicted by the ANSYS Version 10.0 finite element analysis, are summarized to support flaw evaluations of the pressurizer spray nozzle design.

This document is the Non-Proprietary document for 32-9049061-005.

Proprietary information is contained within bold square brackets "**[ ]**".

THE FOLLOWING COMPUTER CODES HAVE BEEN USED IN THIS DOCUMENT:

CODE/VERSION/REV	CODE/VERSION/REV
ANSYS Version 10.0 & Operating System : Not Known (Rev 000 through Rev 003)	ANSYS Version 14.0 & Operating System : Win 7 (Revision 004))

THE DOCUMENT CONTAINS ASSUMPTIONS THAT SHALL BE VERIFIED PRIOR TO USE

☐Yes

☒ No

AREVA

Diablo Canyon Unit 2 Pressurizer Spray Nozzle Weld Overlay Residual Stress Analysis – Non-Proprietary

Review Method: ☒ Design Review (Detailed Check)

☐ Alternate Calculation

Signature Block

Name and Title (printed or typed)	Signature	P/R/A and LP/LR	Date	Pages/Sections Prepared/Reviewed/Approved
Samer H Mahmoud Principal Engineer		P	3/26/14	All.
Silvester J Noronha Principal Engineer		R	3/26/14	All.
Tim M Wiger Engineering Manager		A	3/27/14	All.

Note: P/R/A designates Preparer (P), Reviewer (R), Approver (A);
LP/LR designates Lead Preparer (LP), Lead Reviewer (LR)

Project Manager Approval of Customer References (N/A if not applicable)

Name (printed or typed)	Title (printed or typed)	Signature	Date
N/A	N/A	N/A	N/A

Mentoring Information (not required per 0402-01)

Name (printed or typed)	Title (printed or typed)	Mentor to: (P/R)	Signature	Date
N/A	N/A	N/A	N/A	N/A

Record of Revision

Revision No.	Pages/Sections/Paragraphs Changed	Brief Description / Change Authorization
000	All	Original Release
000	All	Non-Proprietary document for 32-9049061-005

Table of Contents

Page

SIGNATURE BLOCK 2

RECORD OF REVISION 3

LIST OF TABLES 5

LIST OF FIGURES 6

1.0 PURPOSE 7

2.0 ANALYTICAL METHODOLOGY 7

3.0 KEY ASSUMPTIONS 8

4.0 DESIGN INPUT 8

4.1 Geometry 8

4.2 Finite Element Model 8

4.3 Materials 9

4.4 Welding Parameters 10

4.5 Boundary Conditions 10

4.5.1 Thermal Analysis 10

4.5.2 Structural Analysis 10

5.0 FINITE ELEMENT RESULTS/SUMMARY 11

6.0 REFERENCES 12

7.0 COMPUTER OUTPUT 13

8.0 FIGURES SECTION 14

APPENDIX A : AXIAL AND HOOP STRESS TABLES 23

APPENDIX B : VERIFICATION OF THE FINITE ELEMENT PROGRAM 25

APPENDIX C : STRESS FOR EVALUATING NDE INDICATIONS 26

List of Tables

Page

Table 4-1: Dimensions of Spray Nozzle Design and SWOL 8
Table 4-2: Component Material Designation 9
Table 4-3: Welding Parameters 10
Table 7-1: Computer Output Files for Fracture Mechanics Analysis* 13

Table A-1: Through-wall axial and hoop stress distributions at shutdown (70F) 23
Table A-2: Through-wall axial and hoop stress distributions at steady state ([ ] F) 24
Table C-1: Bounding Radial and Shear Stresses for Interfacial Path lines 27
Table C-2: Through-wall axial and hoop stress distributions for vertical path lines at shutdown (70°F) 27
Table C-3: Computer Files 28

List of Figures

Page

Figure 1: Welding of the stainless steel safe end to the pressurizer spray nozzle using Alloy 82/182 weld metal 14

Figure 2: Removal of weld material from the inner surface of the DMW and replacement of the cavity with Alloy 182 weldment to simulate a weld repair 14

Figure 3: Welding of the liner to the inside surface of the nozzle 14

Figure 4: Welding of the stainless steel pipe to the safe end using stainless steel weld metal 14

Figure 5: Welding of an [ ] SWOL onto the outer surface, covering the nozzle, the DMW, and the stainless steel weld 14

Figure 6: Finite element mesh for the spray nozzle design and SWOL 15

Figure 7: Weld passes employed in the DMW 16

Figure 8: Weld passes employed for the weld repair and in the stainless steel weld 16

Figure 9: Weld passes employed in the SWOL and liner weld 16

Figure 10: Axial and hoop stress contours at shutdown (70F) obtained by applying two operating load cycles following the completion of the SWOL 17

Figure 11: Axial and hoop and stress contours at steady state ([ ] F) obtained by applying two-and-a-half operating load cycles following the completion of the SWOL 18

Figure 12: Path lines for axial and hoop WRS distribution along the ID surfaces 19

Figure 13: Path lines for the through-wall axial and hoop WRS distribution in the DMW region and the stainless steel weld 19

Figure 14: Axial and hoop stress distributions along the DMW ID surface at steady state ([ ] F) obtained by applying two-and-a-half operating load cycles following the completion of the SWOL. 20

Figure 15: Axial and hoop stress distributions along the liner weld ID surface at steady state ([ ] F) obtained by applying two-and-a-half operating load cycles following the completion of the SWOL 20

Figure 16: Through-wall axial stress distributions at shutdown (70F) obtained by applying two operating load cycles following the completion of the SWOL 21

Figure 17: Through-wall hoop stress distributions at shutdown (70F) obtained by applying two operating load cycles following the completion of the SWOL 21

Figure 18: Through-wall axial stress distributions at steady state ([ ] F) obtained by applying two-and-a-half operating load cycles following the completion of the SWOL shutdown 22

Figure 19: Through-wall hoop stress distributions at steady state ([ ] F) obtained by applying two-and-a-half operating load cycles following the completion of the SWOL 22

Figure C-1: Spray Nozzle Path Lines 26

1.0 PURPOSE

Alloy 600 and its associated weldments Alloy 82/182 are susceptible to primary water stress corrosion cracking (PWSCC). Pacific Gas and Electric plans to mitigate PWSCC in the Diablo Canyon Unit 2 pressurizer nozzle Alloy 82/182 dissimilar metal weld (DMW) with full structural weld overlays (SWOL) using PWSCC resistant [ ]. The planned mitigation using [ ] SWOL is a preemptive measure to reduce the PWSCC susceptibility of the DMW.

A weld residual stress (WRS) finite element analysis for the pressurizer spray nozzle is performed to develop WRS distributions in support of the fracture mechanics analysis of postulated flaws in the DMW and the stainless steel weld (SSW) between the safe end and piping.

2.0 ANALYTICAL METHODOLOGY

The WRS finite element analysis is carried out per the Reference [1] WRS analysis procedure. The various stages of the welding processes for the structural components, the weld repair, and the SWOL, along with test and operating conditions, are simulated in the finite element analysis using the following sequential steps:

1. Welding of the stainless steel safe end to the pressurizer spray nozzle using Alloy 82/182 weld metal.
2. Removal of weld material from the inner surface of the DMW and replacement of the cavity with Alloy 182 weldment to simulate a weld repair.
3. Welding of the liner to the inside surface of the nozzle.
4. Simulation of hydro test.
5. Welding of the stainless steel pipe to the safe end using a stainless steel weld metal.
6. Simulation of hydro test.
7. Simulation of operational loads.
8. Welding of an [ ] SWOL onto the outer surface, covering the nozzle, the DMW, and the stainless steel weld.
9. Simulation of operational loads.
10.

Figure 1 to Figure 5 illustrate these stages.

The general purpose finite element code ANSYS [2] is used to perform the WRS finite element analysis. The finite element analysis is based on a two-dimensional axisymmetric model. The basic steps comprising the multi-pass welding simulation of the DMW, the weld repair, the stainless steel weld, and the SWOL are as follows:

- Develop the finite element model considering features necessary to accommodate weld pass deposition and weld repairs.
- Define the temperature range for melting (solidus and liquidus temperatures).
- Define thermal and mechanical temperature dependent material properties from room temperature up to and including the melting region.
- Define thermal and structural boundary conditions.
- Define volumetric heat sources from welding procedure specifications.
- Thermal phase using the ANSYS "birth and death" feature
  - Deactivate finite elements in all weld passes.

- Activate one weld pass at a time and perform transient thermal analysis to develop the history of the temperature field for subsequent structural analysis.

- Structural phase using the ANSYS "birth and death" feature
  - Deactivate elements in all weld passes.
  - Activate one weld pass at a time and perform static structural elastic-plastic analysis using the temperature history from the thermal phase.
- Perform additional static load steps to simulate hydrostatic testing, steady state operation, and thermal cycling.

3.0 KEY ASSUMPTIONS

There are no major assumptions for this calculation. Minor assumptions are noted where applicable.

4.0 DESIGN INPUT

4.1 Geometry

The detailed dimensions of the spray nozzle design and SWOL modeled in the WRS finite element analysis are obtained from [3] and [4] and are shown in Table 4-1. The liner weld is modeled larger than what the original configuration drawing [3] represents it to be. The larger liner weld is essentially a large ID weld repair, which would tend to lead to conservatively higher residual stresses in that region.

Table 4-1: Dimensions of Spray Nozzle Design and SWOL

Component	Dimension
Pipe ID	[ ]
Pipe OD	[ ]
Safe End ID at SS Weld	[ ]
Nozzle ID	[ ]
Nozzle OD (near head)	[ ]
Min Weld Overlay Thickness (at nozzle side)	[ ]

4.2 Finite Element Model

The finite element model is a two-dimensional axisymmetric model. The finite element mesh consists of ANSYS four-node thermal (axisymmetric PLANE55) and structural (axisymmetric PLANE182) elements. The B-bar method of selective reduced integration is used for the structural elements in order to avoid mesh locking due to near incompressibility condition at large plastic strains. The weld pass depositions are simulated using ANSYS' element "birth and death" feature.

The finite element mesh for the spray nozzle design and SWOL is shown in Figure 6. The DMW and stainless steel welds are sufficiently separated from the boundaries of the model that the "end effects" do not significantly affect stresses in the welds. The dimensions of the finite element model are developed per drawings [3] and [4]. The weld passes employed in the DMW, the weld repair, the liner weld, the stainless steel weld, and the SWOL are shown in Figure 7, Figure 8, and Figure 9, respectively.

4.3 Materials

Reference [5] provides the component material designation of various components modeled in the WRS analysis, as summarized in Table 4-2.

Table 4-2: Component Material Designation

Component	Material Designation
Nozzle	[ ]
Safe End	[ ]
Nozzle to Safe End Weld	[ ]
Buttering Weld	[ ]
Liner	[ ]
Pipe	[ ]
Safe End to Pipe Weld	[ ]
Weld Overlay	[ ]

The analysis herein uses the physical properties (thermal conductivity, specific heat, mean coefficient of thermal expansion, density, Young's modulus, and Poisson's ratio) and the stress-strain curves from Reference [6] that are representative of the materials in Table 4-2. All of the physical and mechanical properties, except the Poisson's ratio, are temperature dependent.

The multi-linear kinematic hardening model in ANSYS is employed in the elastic-plastic structural analysis. Temperature dependent, true stress-strain material properties are used with the multi-linear kinematic hardening model for simulating the structural phase of the welding procedure.

4.4 Welding Parameters

The welding parameters used in the modeling of the welding processes are shown in Table 4-3.

Table 4-3: Welding Parameters

Welding Parameter	Value

4.5 Boundary Conditions

4.5.1 Thermal Analysis

The thermal model is loaded by a volumetric heat source applied to each weld pass. To enforce thermal continuity with adjacent components, adiabatic boundary conditions are applied at the nozzle end (where it attaches to the vessel) and at the end of the piping section modeled. Thus no heat transfer occurs through the two ends of the model shown in Figure 6. Heat loss at the inner and outer surfaces is simulated using a heat transfer coefficient of [ ] BTU/hr-ft^2-°F per the Reference [1] WRS procedure to model natural convection to an air environment. Radiative boundary conditions are not considered since radiation losses from the molten weld pool are included in the weld efficiency.

4.5.2 Structural Analysis

The temperature history from the thermal analysis is used as the thermal load in the structural analysis. A traction free boundary condition is maintained on all external surfaces of the finite element model. The finite element model is constrained against rigid body translation and rotation by eliminating axial displacements at the nozzle end.

5.0 FINITE ELEMENT RESULTS/SUMMARY

Following the completion of the SWOL simulation, two operating load cycles were applied to the finite element model to obtain a stable state of residual stress to simulate shakedown. This stress state is referred to as shutdown at 70F. The axial and hoop stress contours at shutdown (70F) are shown in Figure 10. Following shutdown at 70F, an additional half cycle of operating loads were applied to the finite element model to obtain the sustained stresses under steady state condition at [ ] F. Figure 11 shows the axial and hoop stress contours at the steady state ([ ] F).

PWSCC is only a concern when the conditions of high temperature, corrodant, and high tensile stress state in a susceptible material are met simultaneously. Alloy 82/182 is a material that is susceptible to PWSCC. The operating temperature of the pressurizer spray nozzle design is conducive to PWSCC.

Figure 14 shows the steady state ([ ] F) axial and hoop stress distributions along a path line ("IDSURF1") at the DMW inner surface. Figure 15 shows the steady state axial and hoop stress distributions along a path line ("IDSURF2") at the inner surface of the liner weld and safe end. These path lines (shown in

Figure 12) includes the surfaces of the nozzle, the butter, the repair weld, the DMW, the liner weld, and the safe end. It is seen that the axial and hoop stresses are all compressive along the inner surface of the DMW region, thus showing the effectiveness of SWOL as a preemptive measure to reduce the PWSCC susceptibility of the DMW.

The through-wall axial and hoop stress distributions, along three path lines in the DMW region and one path line in the SSW, at shutdown (70F) are shown in

Figure 16 and Figure 17, respectively. These path lines are defined in Figure 13. These axial and hoop stress distributions at shutdown (70F) are part of the sources of stress to be used in fatigue crack growth evaluations. They are tabulated in Appendix A.

The through-wall axial and hoop stress distributions at steady state ([ ] F) are given in Figure 18 and Figure 19 respectively, using the same path lines defined in Figure 13. These axial and hoop stress distributions at steady state ([ ] F) are part of the required stress input to the PWSCC crack growth evaluations. They are also tabulated in Appendix A.

As pointed out in Section 4.1, the liner weld has been modeled somewhat larger than described in the original configuration drawing [3]. The larger size produces conservatively higher residual stresses in what is in effect a large ID weld repair. These stresses are highly localized, as evidenced by the stress plots shown in Figure 18 and Figure 19. In these Figures, Path FR_3 is adjacent to the liner weld. A comparison of the inside surface stresses for all three paths FR_1 to FR_3 shows that these stresses are very similar, such that the liner weld does not significantly impact the inside surface stresses along Path FR_3.

Analysis of a similar pressurizer nozzle [8] more closely models the design size of the liner weld. In this analysis, the ID (i.e., wetted) surface of the liner weld presents residual compressive stress, rather than the tensile residual stress predicted in this calculation. While residual tensile stress in the liner weld ID surface is suggestive of susceptibility to PWSCC, the actual stress state in this nozzle is likely to be compressive, as it is in Reference [8], and therefore of little or no susceptibility to PWSCC. In either case, in the unlikely case that the liner weld was to fail, exposure of the underlying low-alloy steel nozzle material to borated reactor coolant water not of concern because of the lack of oxygen in the pressurizer steam space – the boric acid corrosion mechanism is inactive without oxygen.

Additionally, the WRS analysis conservatively assumed that a large inside surface weld repair exists in the DM weld, whereas weld records at Diablo Canyon confirm that is not the case. No weld repairs were made to the inside surface of the DM weld. The effect of the weld repair can be seen in the results shown in Figure 18 and 19 along Path FR_2 which shows significantly higher stresses in the vicinity of the repair than paths FR_1 and FR_3.

6.0 REFERENCES

1. AREVA NP Document 32-2500013-001, "Technical Basis for Numerical Simulation of Welding Residual Stresses."
2. "ANSYS" Finite Element Computer Code, Version 10.0, ANSYS Inc., Canonsburg, PA.
3. AREVA NP Drawing 02-8018400C-002, "Diablo Canyon Unit 2 Pressurizer Spray Nozzle Existing Configuration."
4. AREVA NP Drawing 02-8019233D-001, "Diablo Canyon Pressurizer Spray Nozzle Weld Overlay Design Input."
5. AREVA NP Document 08-9042937-003, "Pressurizer Nozzle Weld Overlays at Pacific Gas and Electric Diablo Canyon Nuclear Power Plant, Unit 2 – Certified Design Specification"
6. AREVA NP Document 32-2500012-002, "Materials Database for Weld Residual Stress Finite Element Analyses."
7. AREVA NP Document 55-WP3-8-F43OLTBSCa3-005, "Welding Procedure Specification."
8. AREVA NP Document 32-9049062-004, "Diablo Canyon Unit 2 Pressurizer Safety/Relief Nozzle Weld Overlay Residual Stress Analysis."

7.0 COMPUTER OUTPUT

The computer output files that support the fracture mechanics analysis are listed in Table 7-1.

Table 7-1: Computer Output Files for Fracture Mechanics Analysis*

File Name	Date	Description
SDAXIAL.out	5-23-2007	Axial stress along all four path lines at shutdown (70F)
SDHoop.out	5-23-2007	Hoop stress along all four path lines at shutdown (70F)
SDLocs.out	5-23-2007	Path coordinates for all four path lines at shutdown (70F)
SDLocX.out	5-23-2007	Path x coordinates for all four path lines at shutdown (70F)
SDLocY.out	5-23-2007	Path y coordinates for all four path lines at shutdown (70F)
OCAXIAL.out	5-23-2007	Axial stress along all four path lines at steady state ([ ] F)
OCHoop.out	5-23-2007	Hoop stress along all four path lines at steady state ([ ] F)
OCLocs.out	5-23-2007	Path coordinates for all four path lines at steady state ([ ] F)
OCLocX.out	5-23-2007	Path x coordinates for all four path lines at steady state ([ ] F)
OCLocY.out	5-23-2007	Path y coordinates for all four path lines at steady state ([ ] F)
vm32-Modified.vrt	5-22-2007	Axisymmetric analysis of thermal stresses in an infinitely long cylinder. Verification Case for elements PLANE55 and PLANE182.
vm38-Modified.vrt	5-22-2007	Axisymmetric analysis of elastic plastic problem of an infinitely long cylinder under pressure. Verification Case for element Plane182.

*** Note: The computer output from Revision 000 of this document is unchanged and remains applicable to Revision 003. It is therefore not attached to Revision 003. The list of computer output is provided for information only.**

8.0 FIGURES SECTION

Figure 1: Welding of the stainless steel safe end to the pressurizer spray nozzle using Alloy 82/182 weld metal

Figure 2: Removal of weld material from the inner surface of the DMW and replacement of the cavity with Alloy 182 weldment to simulate a weld repair

Figure 3: Welding of the liner to the inside surface of the nozzle

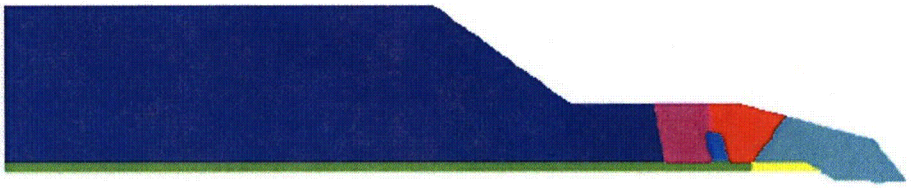

Figure 4: Welding of the stainless steel pipe to the safe end using stainless steel weld metal

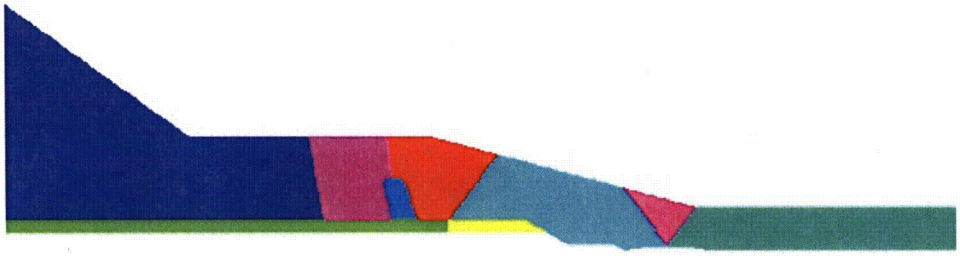

Figure 5: Welding of an [ ] SWOL onto the outer surface, covering the nozzle, the DMW, and the stainless steel weld

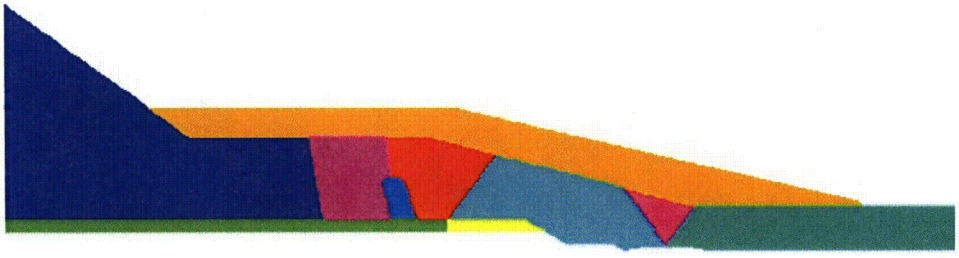

Figure 6: Finite element mesh for the spray nozzle design and SWOL

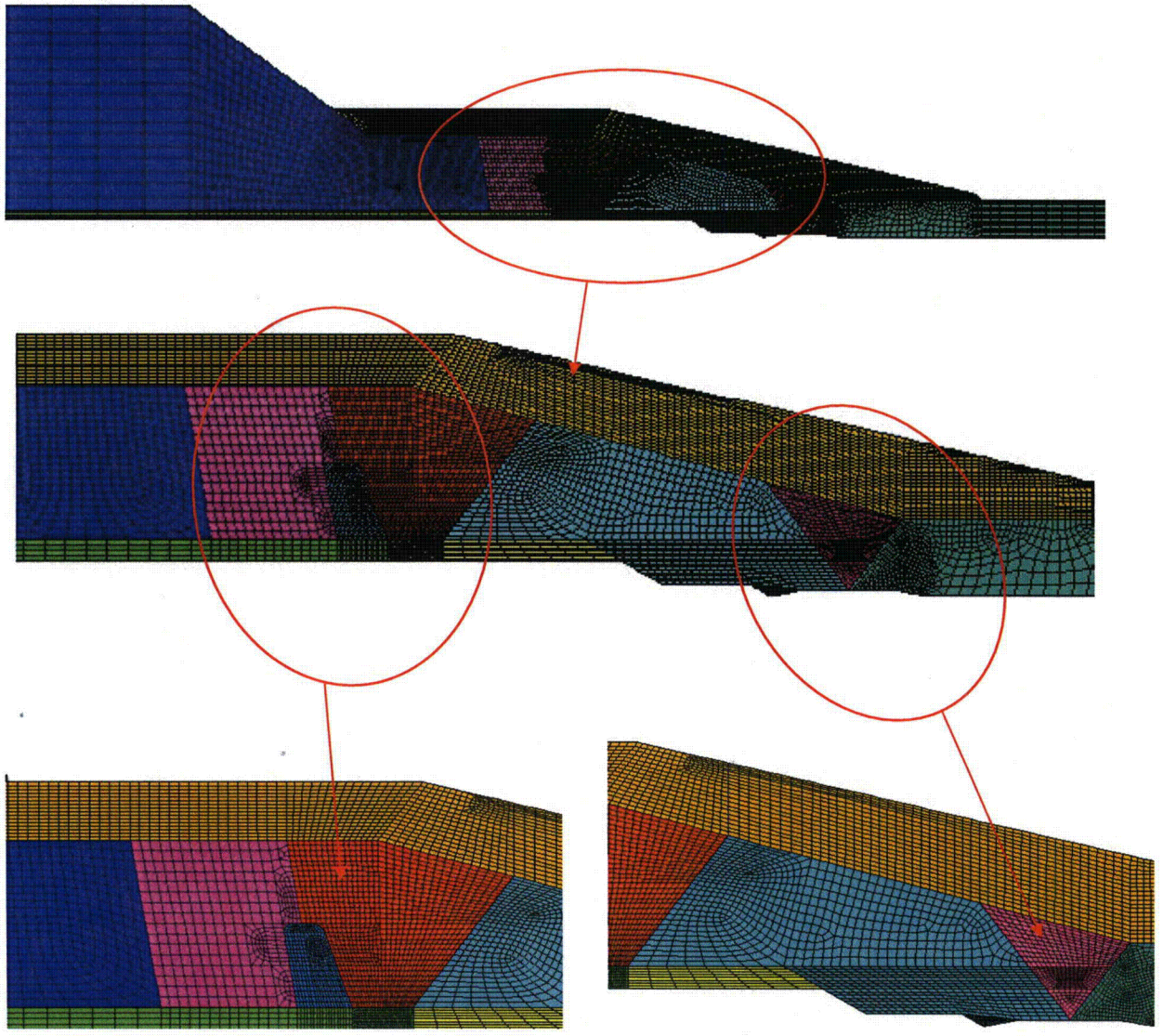

DM Weld with Repair

Stainless Steel Weld

Figure 7: Weld passes employed in the DMW

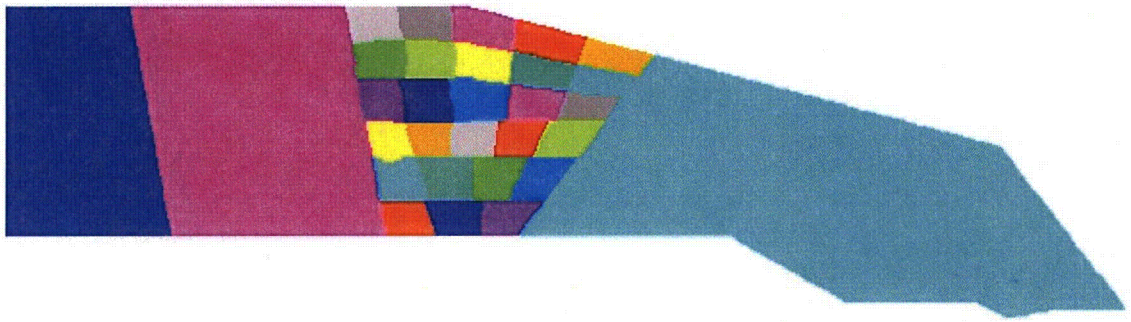

Figure 8: Weld passes employed for the weld repair and in the stainless steel weld

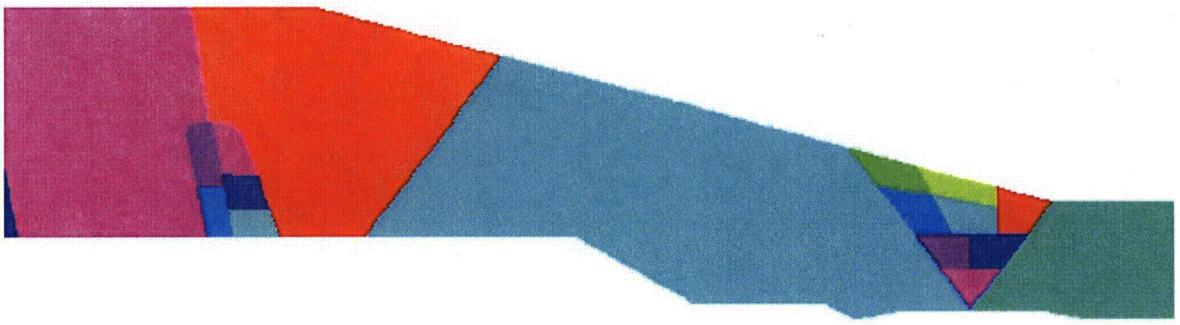

Figure 9: Weld passes employed in the SWOL and liner weld

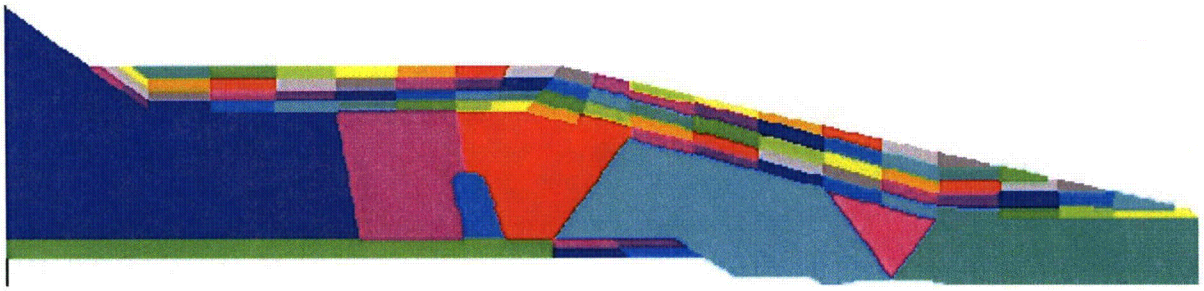

Figure 10: Axial and hoop stress contours at shutdown (70F) obtained by applying two operating load cycles following the completion of the SWOL

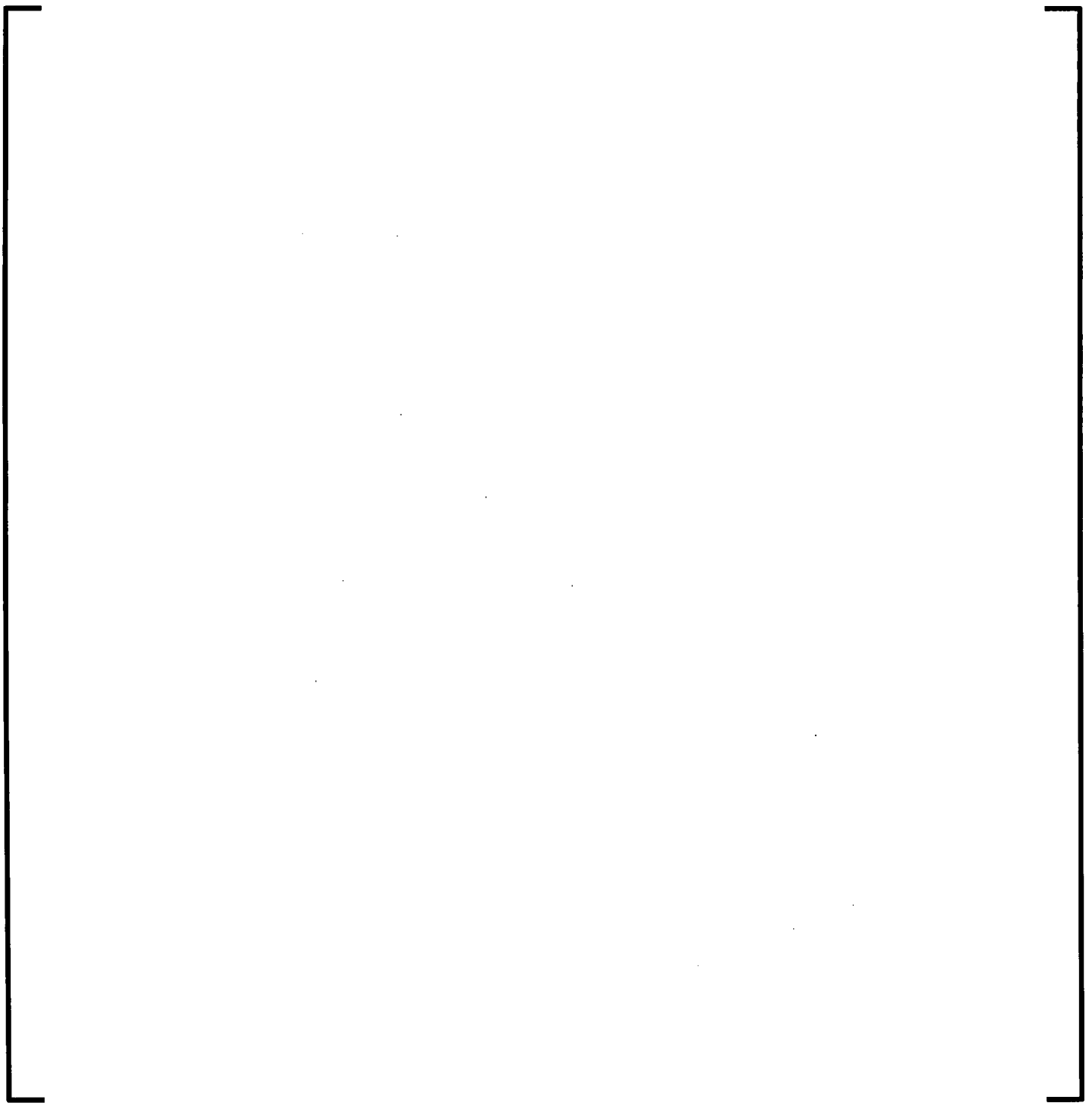

Figure 11: Axial and hoop and stress contours at steady state ([ ] F) obtained by applying two-and-a-half operating load cycles following the completion of the SWOL

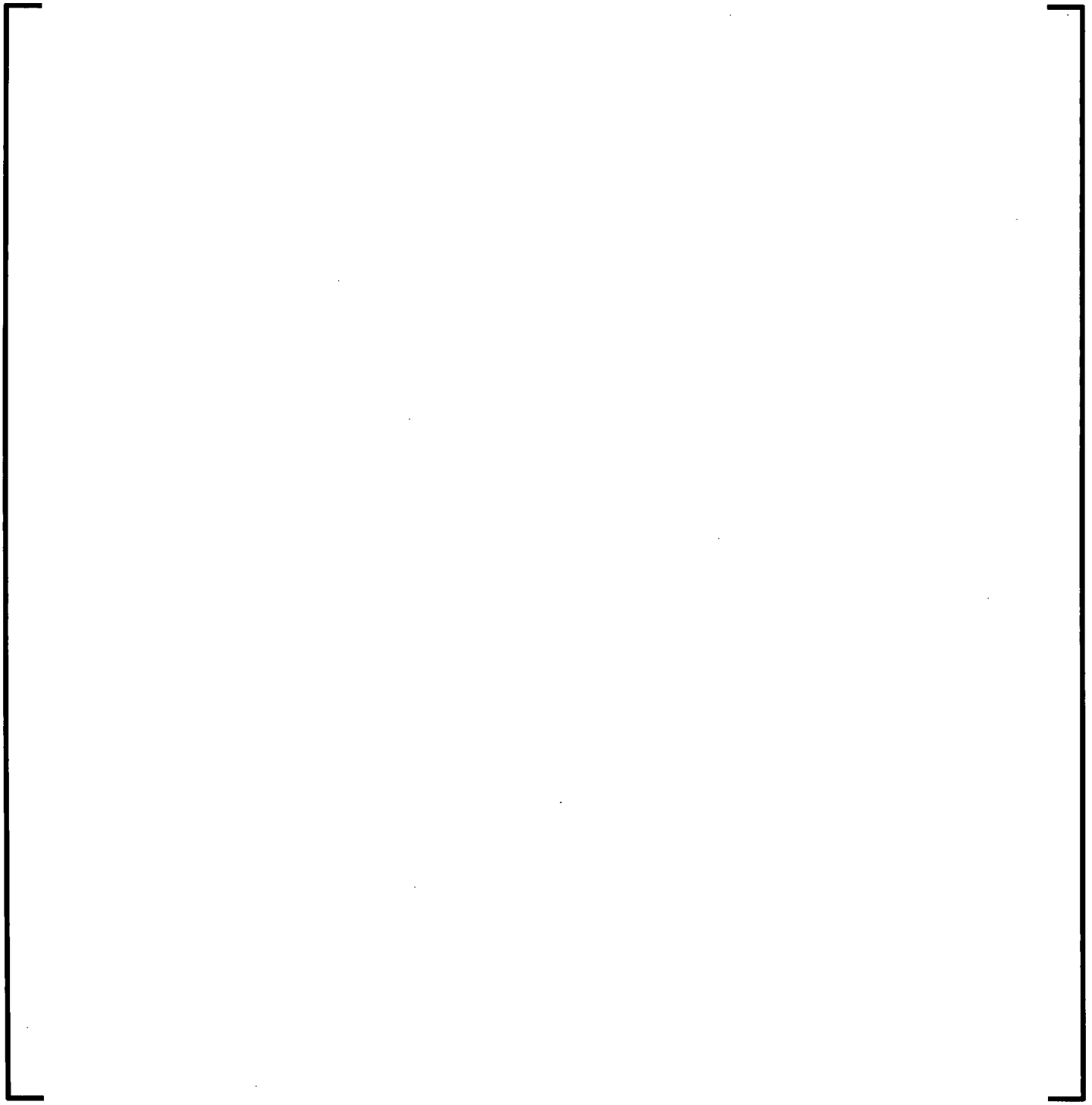

Figure 12: Path lines for axial and hoop WRS distribution along the ID surfaces

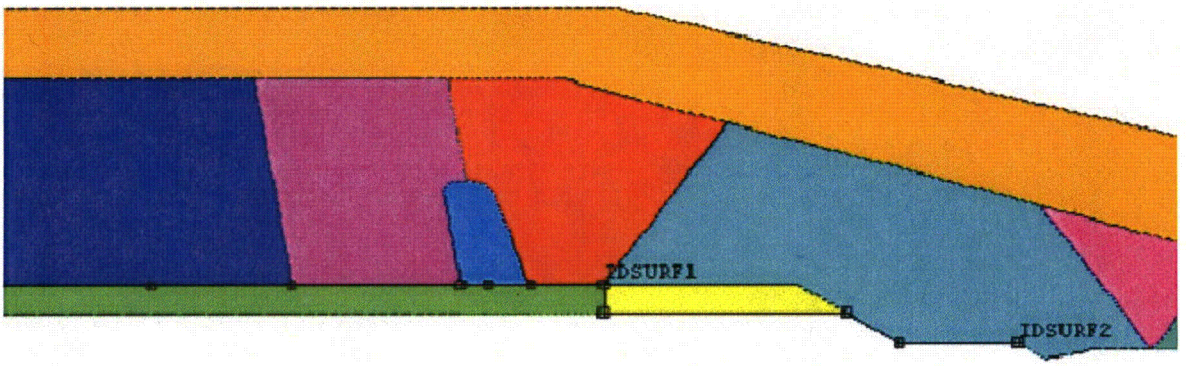

Figure 13: Path lines for the through-wall axial and hoop WRS distribution in the DMW region and the stainless steel weld

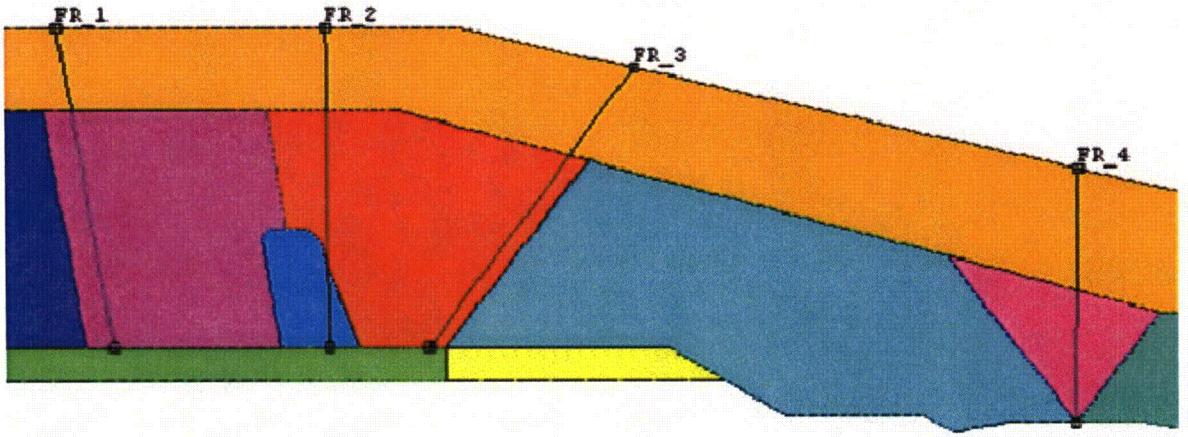

Figure 14: Axial and hoop stress distributions along the DMW ID surface at steady state ([ ] F) obtained by applying two-and-a-half operating load cycles following the completion of the SWOL

[ ]

Figure 15: Axial and hoop stress distributions along the liner weld ID surface at steady state ([ ] F) obtained by applying two-and-a-half operating load cycles following the completion of the SWOL

[ ]

Figure 16: Through-wall axial stress distributions at shutdown (70F) obtained by applying two operating load cycles following the completion of the SWOL

Figure 17: Through-wall hoop stress distributions at shutdown (70F) obtained by applying two operating load cycles following the completion of the SWOL

Figure 18: Through-wall axial stress distributions at steady state ([ ] F) obtained by applying two-and-a-half operating load cycles following the completion of the SWOL shutdown

Figure 19: Through-wall hoop stress distributions at steady state ([ ] F) obtained by applying two-and-a-half operating load cycles following the completion of the SWOL

APPENDIX A: AXIAL AND HOOP STRESS TABLES

Figure 13 shows the path lines along which the stress results are obtained. The axial and hoop WRS distribution at the completion of the SWOL at shutdown and steady state operating conditions are listed in Table A-1 and Table A-2 respectively.

Table A-1: Through-wall axial and hoop stress distributions at shutdown (70F)

Along Path Line "FR_1"		
Distance Along Path Line from the ID (in.)	**Axial WRS (psi)**	**Hoop WRS (psi)**

Along Path Line "FR_2"		
Distance Along Path Line from the ID (in.)	**Axial WRS (psi)**	**Hoop WRS (psi)**

Along Path Line "FR_3"		
Distance Along Path Line from the ID (in.)	**Axial WRS (psi)**	**Hoop WRS (psi)**

Along Path Line "FR_4"		
Distance Along Path Line from the ID (in.)	**Axial WRS (psi)**	**Hoop WRS (psi)**

Table A-2: Through-wall axial and hoop stress distributions at steady state ([ ] F)

Along Path Line "FR_1"		
Distance Along Path Line from the ID (in.)	**Axial WRS (psi)**	**Hoop WRS (psi)**

Along Path Line "FR_2"		
Distance Along Path Line from the ID (in.)	**Axial WRS (psi)**	**Hoop WRS (psi)**

Along Path Line "FR_3"		
Distance Along Path Line from the ID (in.)	**Axial WRS (psi)**	**Hoop WRS (psi)**

Along Path Line "FR_4"		
Distance Along Path Line from the ID (in.)	**Axial WRS (psi)**	**Hoop WRS (psi)**

APPENDIX B: VERIFICATION OF THE FINITE ELEMENT PROGRAM

The following two verification cases were run to verify that the finite element program ANSYS [2] executes properly. The two cases were selected to verify the elements used in the current analysis (plane 55 and plane 182) for the scope of the simulations used in this document, thermal stress analysis in an infinitely long cylinder and elastic plastic structural analysis in a cylinder. For the thermal stress analysis case, the standard ANSYS verification case (vm32) is setup to verify plane 55 (thermal) and plane 42 (structural). This case was modified to replace plane 42 structural element with plane 182. For the elastic plastic case, the ANSYS verification test case was setup to handle plane 42, this case was modified to verify the plane 182 element instead of the plane 42 structural element. The results of the verification cases are presented below:

---------- VM32-Modified RESULTS COMPARISON ----------

	TARGET	ANSYS	RATIO
THERMAL ANALYSIS:			
T (C) X=.1875 in	-1.00000	-1.00000	1.000
T (C) X=.2788 in	-0.67037	-0.67039	1.000
T (C) X=0.625 in	0.00000	0.00000	0.000
PRINTOUT RESUMED BY /GOP			
STATIC ANALYSIS:			
A_STS psi X=.187	420.42	429.99	1.023
T_STS psi X=.187	420.42	429.61	1.022
A_STS psi X=.625	-194.58	-205.15	1.054
T_STS psi X=.625	-194.58	-205.08	1.054

---------- VM38-Modified RESULTS COMPARISON ----------

	TARGET	ANSYS	RATIO
FULLY ELASTIC, PLANE182 RESULTS:			
SIGR LFT_END psi	-9984.	-10075.	1.009
SIGT LFT_END psi	18645.	18785.	1.008
SIGR RT_END psi	-468.	-478.	1.021
SIGT RT_END psi	9128.	9131.	1.000

FULLY PLASTIC, PLANE182 RESULTS:

SIGEFF L	30000.	31239.	1.041
SIGEFF R	30000.	30442.	1.015

This is modified from ANSYS VM38 case to verity the PLANE182
Element solving a problem of Long Cylinder under plastic
Pressure Load

APPENDIX C: STRESS FOR EVALUATING NDE INDICATIONS

C.1 Purpose

The purpose of this appendix is to summarize residual stresses to support flaw evaluations of indications detected or assumed to exist based on the results of the 2013 seventeenth refueling outage (2R17) inservice inspection that are considered rejectable in the overlaid Pressurizer (PZR) Spray Nozzles of Diablo Canyon Power Plant (DCPP) Unit 2. The indications are reported in Reference [C1]. Results are provided along pathlines that are located in close proximity to the found indications in the Spray nozzle.

C.2 Methodology

This revision provided only post processing of the database that was developed in the previous revision of the document. Path lines for obtaining the residual stresses were selected to best match the locations and sizes of the flaw indications as described in Reference [C1]. It should be noted that since the finite element is discrete and it does not exactly match the sketches of the Spray Nozzles provided in Reference [C1], the selected path lines location and sizes are only a best estimate representation of the indications locations and sizes. For every reportable indications two path lines were selected, an interfacial (horizontal path line) and a vertical path line. The interfacial path line is used to sample stresses to be used for evaluating a laminar flaw. Thus radial and shear stresses are of interest for the interfacial path line. The vertical path line is used to sample stresses to be used for evaluation any planar projection of the indications. Axial, hoop stresses, or both axial and hoop stresses may be used for evaluating the planar extent of the indications. The pathlines investigated in this appendix are illustrated in Figure C-1. Note that all reported indications in the Spray nozzle were laminar. Thus only the pathline along the interface between the nozzle and weld overlay (pathline 1) and the pathline along the interface between the safe end to pipe weld and the weld overlay (pathline 2) are need for flaw evolution of the reported indications in the Spray nozzle. The vertical pathlines in Figure C-1 (pathlines 1v and 2v) are included for information only since they are not needed for flaw evaluations.

Figure C-1: Spray Nozzle Path Lines

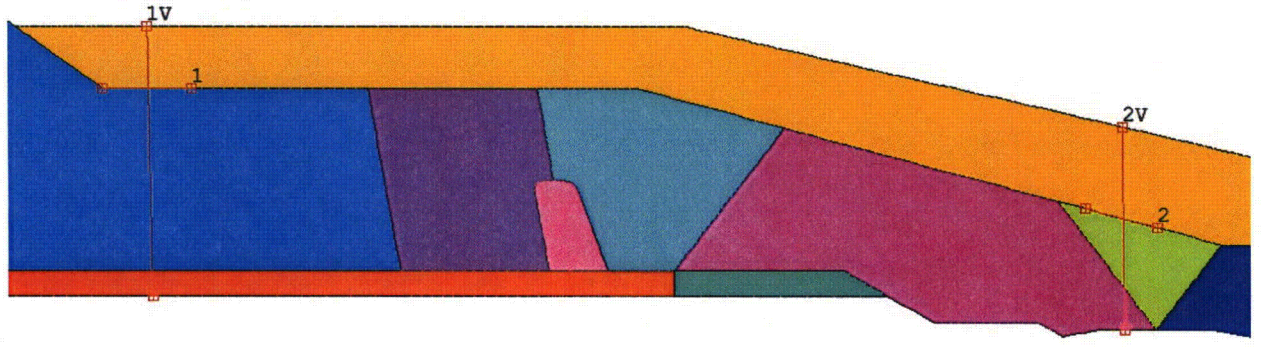

C.3 Results

Axial (SY), hoop (SZ), radial (SX), and shear (SXY) stresses are read from the database and the result files that were archived with the previous revisions of this document. To ensure that the stress sampling results in the most bounding stresses for the path lines located near the interface of the overlay and the original material (nozzle), the post processing for interfacial path lines was processed while selecting either the overlay material, the nozzle material, or both materials.

C.3.1 Interfacial Path lines Results

As mentioned above, the interfacial path lines are of interest for evaluating laminar flaws. Thus, only the radial and shear stresses are of interests. As discussed before, for all interfacial paths, the post processing runs were performed by either selecting all materials, overlay material, or nozzle material. The results are documented in output files "Spray_pathsALL.out", "Spray_pathsOL.out" and "Spray_pathsBASE.out". The results from the output files are manipulated in files "Results.xlsm" to select most bounding stresses. The minimum and maximum values of the radial and shear stresses are tabulated in Table C-1.

Table C-1: Bounding Radial and Shear Stresses for Interfacial Path lines

Nozzle	Radial Stress (psi)		Shear Stress (psi)	
	Minimum	Maximum	Minimum	Maximum
Spray Nozzle (1)	[ ]	[ ]	[ ]	[ ]
Spray Nozzle (2)	[ ]	[ ]	[ ]	[ ]

C.3.2 Vertical Path lines Results

All reported indications in the Spray nozzle were laminar. Thus only the interfacial pathlines along the interface between weld overlay and the underlying materials (Pathlines 1 and 2 in Figure C-1) are needed for flaw evaluations. The vertical pathlines (Pathlines 1v and 2v in Figure C-1) are included for information only since they are not needed for flaw evaluations. Vertical pathlines are typically required for analyzing planar flaws where only axial and hoop stresses are of interest in the analysis. The post processing was performed by selecting all materials. The results are documented in output files "Spray_pathsALL.out". The hoop and axial stresses are tabulated below in Table C-2.

Table C-2: Through-wall axial and hoop stress distributions for vertical path lines at shutdown (70°F)

Along Path Line "1V"			Along Path Line "2V"		
Distance Along Path Line from the ID (in.)	**Hoop WRS (psi)**	**Axial WRS (psi)**	**Distance Along Path Line from the ID (in.)**	**Hoop WRS (psi)**	**Axial WRS (psi)**
[ ]					

C.4 Computer Usage

C.4.1 Software and Hardware

ANSYS Version 14.0 [C2] was used in this calculation. Verification test cases were performed and documented herein.

- Computer program tested: ANSYS Version 14.0, verification tests vm32mod2D.vrt and vm38mod2D.vrt.
- Error notices for ANSYS Version 14.0 were reviewed and none apply for this analysis.
- Computer hardware used: The computer hardware used in the analysis is DELL (Service Tag # 5VKW5S1). The hardware platform is Intel® Core™ i7-2640M CPU @ 2.8 GHz, 8 GB RAM and operating system is Microsoft Windows 7 Enterprise x 64 Edition, Version 2009, and Service Pack 1.
- Name of person running the test: Silvester Noronha
- Date of test: 11-05-2013
- Acceptability: For ANSYS 14.0 cases vm32mod2D, vm38mod2D, obtained from Reference [1] are run to verify that the answers are correct. The files vm32mod2D.vrt and vm38mod2D.vrt contain output from the test cases. Review of the output shows that the answers are identical to those contained in Reference [1].

C.4.2 Computer Files

All ANSYS input/output files are collected and listed in Table C-3. All computer runs and post processing along with post processing macros are documented in the ColdStor storage path "\cold\General-Access\32\32-9000000\32-9049061-004\official". ANSYS verification input/output files are also listed.

Table C-3: Computer Files

Name	Size	Date/Time Modified	Checksum
PostProcess_SprayALL.inp	4050	Nov 08 2013 15:43:28	61422
PostProcess_SprayOL.inp	4055	Nov 13 2013 09:22:33	48955
PostProcess_SprayBASE.inp	4048	Nov 13 2013 09:15:17	29056
Spray_pathsALL.out	5578	Nov 08 2013 15:44:24	25282
Spray_pathsOL.out	5578	Nov 13 2013 09:22:55	33218
Spray_pathsBASE.out	5578	Nov 13 2013 09:15:50	14784
Results.xlsm	29323	Nov 13 2013 15:00:46	13234
vm32mod2D.inp	3551	Jan 05 2009 10:09:26	30336
vm32mod2D.vrt	624	Nov 05 2013 09:55:59	17780
vm38mod2D.inp	2458	Jan 07 2009 11:28:06	51869
vm38mod2D.vrt	650	Nov 05 2013 09:56:31	36343

C.5 References

C.1. AREVA Document 38-9200149-001, (DCPP Unit 2 DIT-50540188-04-00), "DCPP Unit 2 Pressurizer Nozzle NDE Data."

C.2. ANSYS Finite Element Computer Code, Version 14.0, ANSYS Inc., Canonsburg, PA